Molecular Dynamics Investigation of Adhesion between TATB Surfaces and Amorphous Fluoropolymers

Richard H. Gee,* Amitesh Maiti, Sorin Bastea, and Laurence E. Fried

Chemistry, Materials, and Life Science Directorate, Lawrence Livermore National Laboratory, University of California, P.O. Box 808, L-268, Livermore, California 94551

Received January 29, 2007; Revised Manuscript Received March 7, 2007

ABSTRACT: Atomistic simulations are used to study the adhesion properties of amorphous perfluoro- and fluoropolymers onto two different crystal surfaces of 1,3,5-triamino-2,4,6-trinitrobenzene (TATB). Properties of the bulk amorphous polymer melts are also investigated. The fluoropolymers studied in this article include Kel-F 800, Teflon AF, Hyflon AD, and Cytop. Simulations of the bulk polymer melts were performed over a wide range of temperatures including the volumetric glass transition temperature, so as to validate the interaction parameters used. The computed glass transition temperatures and densities compare well with experiment. The solubility parameters for the various polymers also compare well with calculations based on group additive methods. The local molecular structure at the TATB interface as well as the degree of adhesion varies from one polymer to another. All polymers except Hyflon show a propensity to readily wet the two TATB surfaces studied.

I. Introduction

Fluoropolymers have many interesting properties not found in their hydrocarbon analogues.[1] These properties include low surface tension and coefficient of friction, novel piezoelectric and pyroelectric properties, low refractive index, and high chemical and thermal stabilities. Many fluoropolymers also demonstrate an unusually high density, high chemical stability, and mechanical properties suitable for use in the manufacture of pressed powder composites.[2] Furthermore, recently developed amorphous perfluorinated polymers have received increasing attention due to improved creep and adhesive properties.[3−5] Such properties make these polymers ideal candidates for use as binder materials in energetic material formulations, known as plastic-bonded explosives (PBX). Typical PBX formulations have 5−10% polymer binder, which is assumed to coat the remaining solid energetic material particles.[6] Thus, good adhesion to the crystalline energetic material is of fundamental importance in providing safe, low-sensitivity PBX formulations.

Relatively few theoretical studies of the adhesion properties of PBXs have been reported in the literature.[7−14] To this end, we investigate the adhesion of various fluoropolymers to two different crystal surfaces of the energetic material 1,3,5-triamino-2,4,6-trinitrobenzene (TATB) using molecular dynamic simulations (MD). Computer simulations have played an important role in investigating specific interactions between molecules.[15−21] Such studies are of obvious importance in determining the degree of adhesion, which to our knowledge has not been investigated for the polymers studied here.

In this paper four different fluoropolymers melts are studied: Teflon AF 1600 (AF), Cytop (Cytop), Hyflon AD 60 (Hyflon), and Kel-F 800 (Kel-F), where abbreviated names are in parentheses. These polymers are simulated in contact with two different TATB crystal surfaces: [100] and [001].

II. Computational Method

a. The Polymer Representation and Amorphous Cells. The MD simulations of the various fluoropolymers were carried out on a variety of bulk amorphous ensembles as well as ensembles in which amorphous films of each of the four separate fluoropolymers are interfaced to either a [001] or a [100] surface of a TATB crystal.

The bulk amorphous simulations were performed on ensembles consisting of 15 chains composed of 120 total monomer units per chain, for each of the four fluoropolymers studied. The Cytop fluoropolymer chains used in the simulations are composed of monomers shown in Figure 1a. The remaining three fluoropolymers are copolymers. Teflon AF 1600 copolymer chains were obtained by the simulated copolymerization of tetrafluoroethylene (TFE) monomer (35% mole fraction) and 2,2-bis(trifluoromethyl)-4,5-difluoro-1,3-dioxole monomer (65% mole fraction) (Figure 1b); Hyflon AD 60 copolymer chains were obtained by the simulated copolymerization of TFE monomer (40% mole fraction) and 2,2,4-trifluoro-5-fluoromethoxy-1,3-dioxole monomer (60% mole fraction) (Figure 1c); and Kel-F 800 copolymer chains were obtained by the simulated copolymerization of chlorotrifluoroethylene and vinylidene fluoride monomers in a 3:1 mole ratio (Figure 1d).

The initial starting polymer configurations for simulations in the bulk were generated using a Monte Carlo method.[22] The AF, Cytop, and Hyflon monomers were allowed to "polymerize" in a head-to-tail manner with no monomer reversals, resulting in the mole ratios referred to above, while the KelF monomers were allowed to "polymerize" according to the procedure described in ref 23. Additionally, each of the 15 polymer chains was polymerized independently, thus providing a greater statistical representation of the bulk melts. The initial atomic positions of the amorphous melt structures were generated using a random distribution of torsional angles, which was generated using a Monte Carlo method that assigns random values to all rotatable torsions in the polymer chain. The resulting amorphous structure was then relaxed by energy minimization. Bulk simulations were carried out using cubic periodic boundary conditions. All atoms in the polymer chains were treated explicitly.

b. TATB Interfaces. Each of the four fluoropolymers was interfaced to either a [001] or a [100] TATB surface.[24] The TATB surfaces were constructed by first creating an orthogonal bulk supercell from the experimental TATB unit cell and then placing a vacuum normal to the defined surface. We used a

* To whom correspondence should be addressed. E-mail: gee10@llnl.gov.

10.1021/ma0702501 CCC: $37.00
Published on Web 04/03/2007

Table 1. Glass Transition Temperatures, Densities, and Solubility Parameters of Various Fluoropolymers and TATB

	T_g (°C)		ρ (g/cm^3) at 298 K[a]			δ (J/cm^3)$^{1/2}$ at 298 K[c]	
	exp	MD	exp	MD	Synthia	MD	van Krevelen[d]
KelF 800	22−34	18	2.00	1.91	1.93	16.1 [14.8−16.2][b]	16.3
Cytop	108	110	2.03	1.96	2.085	12.8	13.2
Hyflon AD 60	110−121	115	1.93	1.97	2.047	13.3	14.4
AF 1600	160	160	1.814	1.86	2.065	13.9	13.8
TATB			1.937	1.938			

[a] Average cell dimensions of KelF, Cytop, Hyflon, and AF from MD simulations are 68.44, 59.67, 62.70, and 68.13 Å, respectively. [b] Experimental range for poly(chlorotrifluoroethylene) (Cady et al.). [c] $\delta = (\Delta E/V)^{1/2}$, where V is the molar volume and ΔE is the nonbonded potential energy difference between the bulk melt state and that in which the macromolecules can no longer feel each other. [d] Reference 48.

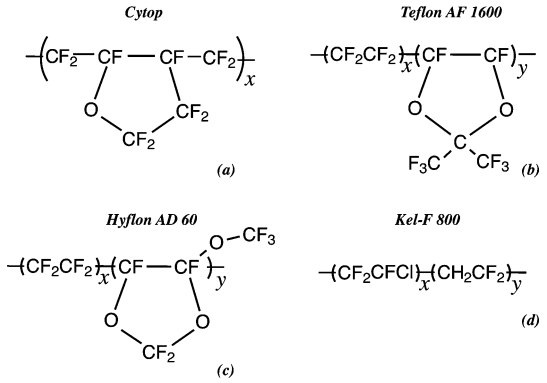

Figure 1. Monomer chemical structures of Cytop (a), Teflon AF (b), Hyflon AD (c), and Kel-F 800 (d).

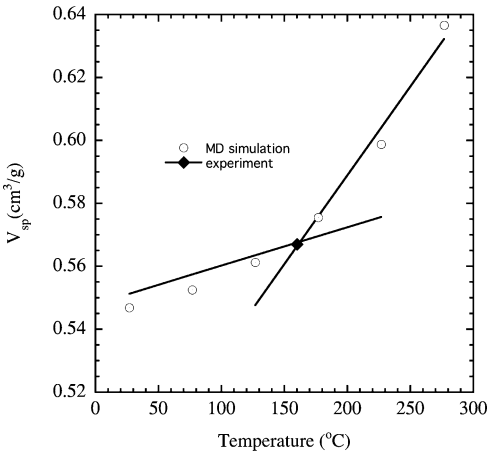

Figure 2. Specific volume vs temperature for AF at 1 atm as determined from *NPT* dynamics. MD results are shown by open symbols (circles); experimental values for T_g (solid diamond) and experimentally determined coefficient of thermal expansion (solid lines) are also shown.[47]

bulk supercell of dimensions $a = 54.1386$ Å, $b = 46.8570$ Å, and $c = 43.9561$ Å, consisting of 504 TATB molecules (12 096 total atoms). All TATB molecules were held fixed in the simulations. For all fluoropolymer/TATB interface simulations, the cell dimension normal to the [001] or [100] TATB interface was extended such that the density of the fluoropolymer at the TATB surface was equal to the equilibrium bulk density at 500 K,[25] as determined from the simulations of the bulk amorphous fluoropolymer melts; the remaining two axis dimensions were fixed ($a = 54.1386$ Å and $b = 46.8570$ Å for the [001] TATB interface; $b = 46.8570$ Å and $c = 43.9561$ Å for the [100] TATB interface). Each of the four different equilibrated amorphous polymer melts (equilibrated at 500 K) was placed at either of the [001] or [100] TATB surfaces, so as to render a melt phase consisting of 15 polymer chains, adjacent to the TATB surface of interest. The ensembles thus created were allowed to equilibrate via *NVT* dynamics for a minimum of

Table 2. Summary of Surface Tension, γ, Work of Adhesion, W_{12}, Interfacial Tension, γ_{12}, and Spreading Coefficient, S, for Various Fluoropolymers (γ_2) Interfaced to TATB (γ_1) in (erg cm^{-2})

	γ_1	γ_2^{MP} [a]	W_{12}	γ_{12}	S
		Interface [001]			
KelF	+66	+27	+76	+17 ± 1	+22
Cytop	+66	+24	+74	+16 ± 2	+26
AF	+66	+23	+78	+11 ± 1	+37
Hyflon	+66	+22	+5	+83 ± 2	-39
		Interface [100]			
KelF	+208	+27	+271	-36 ± 2	+217
Cytop	+208	+24	+275	-43 ± 1	+227
AF	+208	+23	+281	-50 ± 1	+235
Hyflon	+208	+22	+320	-90 ± 1	+276

[a] γ_2^{MP} = surface tension determined from the molar parachor group additive method at 500 K; all other quantities were derived from the MD simulations as described in the text.

2 ns. A data collection period of a minimum of 2 ns and up to greater than 10 ns was used. The orthorhombic cell dimensions of the [001] TATB interface for AF, Cytop, Hyflon, and KelF were $c = 182.9$, 137.64, 148.822, and 190.0 Å, respectively. The orthorhombic cell dimensions of the [100] TATB interface for AF, Cytop, Hyflon, and KelF were $a = 225.185$, 169.528, 183.296, and 233.028 Å, respectively.

c. Potential Functions. The MD simulations of the amorphous bulk fluoropolymer melts employed the COMPASS[26] force field parameter set. The COMPASS potential consists of valence terms including diagonal and off-diagonal coupling terms and nonbonded van der Waals (vdW) and Coulombic interaction terms. The functional form of the potential employs a quartic polynomial for bond stretching and angle bending and a three-term Fourier expansion for torsions. The atomic charges for the nonbonded Coulombic interaction are those parametrized by Sun et al.[26] The vdW interactions are implemented using the well-known Lennard-Jones (LJ) potential and make use of an inverse 9th-power term for the repulsive part rather than the more customary 12th-power term. All valence degrees of freedom were explicitly treated and unconstrained.

The interaction potentials used to treat the explicit crystalline TATB employed our recently developed force field parameter set,[16] except that the vdW interactions were implemented using the LJ 9−6 potential. Further, all unlike atom pairs were determined using the 6th-order combination law.[27]

d. Molecular Dynamics Method. The simulations of all bulk amorphous polymer melts were carried out using constant particle number, pressure, and temperature (*NPT*) dynamics at a pressure of 1 atm, using three-dimensional periodic boundary conditions. Simulations of the polymer/TATB interfaces were performed at a temperature of 500 K[25] using constant particle number, volume, and temperature (*NVT*) dynamics. All computations were carried out using the LAMMPS code.[28] The equations of motion were integrated using the Verlet algorithm[29] with a time step of 1.0 fs. A Nosé-Hoover thermostat[30] with a relaxation time of 0.1 ps was used to control the temperature,

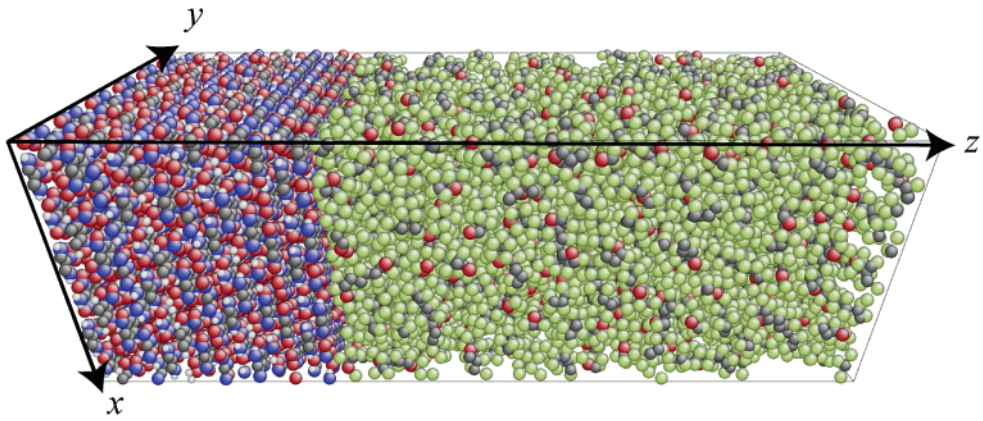

Figure 3. Typical [001] TATB/polymer interface used in the MD simulations.

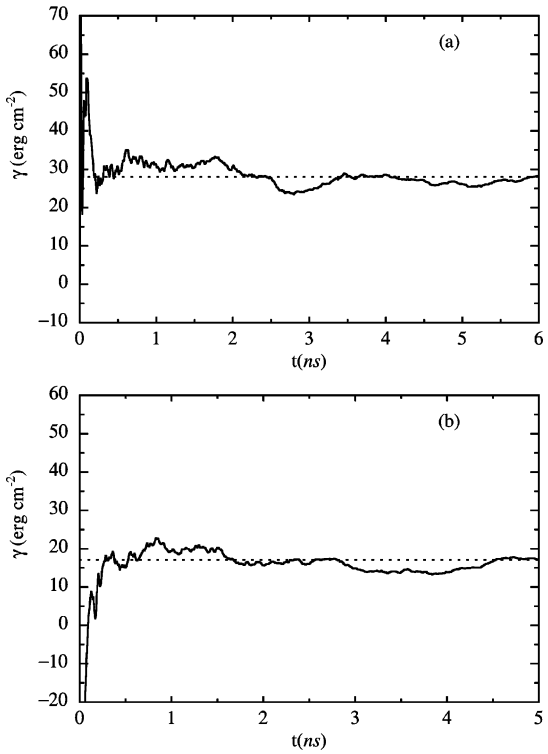

Figure 4. Accumulated averages for the surface tension of a 15 polymer chain KelF film (a) and interfacial surface tension of KelF at the [001] TATB surface (as illustrated in Figure 3) (b) from molecular dynamics. The curves are from simulations, and the dotted line is their average values.

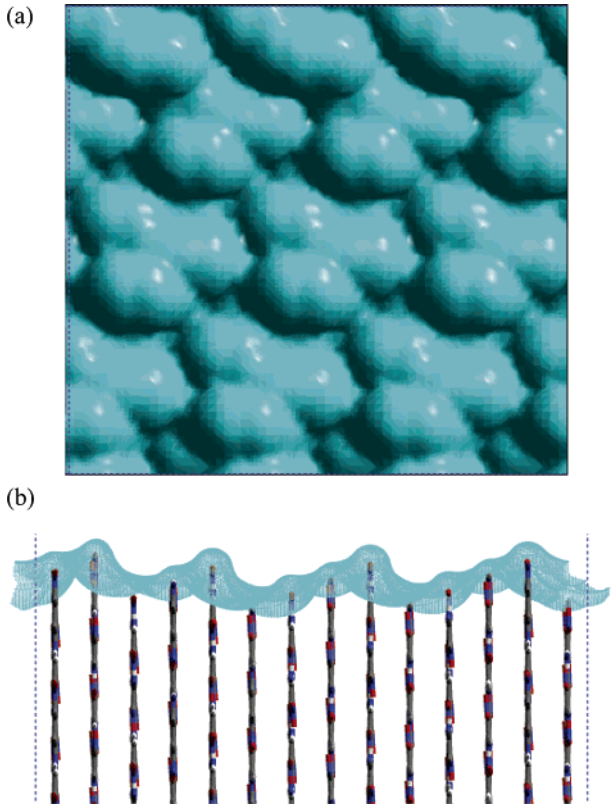

Figure 5. Illustration of the rough [100] TATB Connolly surface, normal to the interfacial surface (a) and perpendicular to the interface (b).

and the pressure was controlled isotropically.[31] The nonbonded vdW interactions were treated by truncating atom pairs with an interatomic distance greater than $r_c = 20$ Å, coupled with a long-range tail correction.[32] The particle−particle particle−mesh Ewald (PPPM) method[33] was used for the long-range treatment of electrostatic interactions. The truncation of Lennard-Jones interactions is known to lead to a dependence of the surface tension of vapor−liquid interfaces on the cutoff radius if this radius is not large enough.[34] The effect also appears to be important for polymer melt interfaces.[35] To avoid such problems, we used a cutoff radius r_c of 20 Å, which is at least 5 times larger than the Lennard-Jones sigma values. By employing different cutoff radii, we also checked that this truncation distance places our surface tension calculations well into the asymptotic regime, where no dependence on r_c is present.

Electrostatic interactions pose subtle difficulties to the calculation of interface properties since the system is not periodic in the direction perpendicular to the interface and computational methods such as Ewald summation generally assume 3D periodic boundary conditions.[36] This can lead to spurious results due to the interactions between the periodic images perpendicular to the interface. However, such effects are important for systems that contain free charges or dipoles and where surface polarization effects are important. This is not the case for the system studied here, which is strongly screened locally and which exhibits minimal polarization behavior. To ensure computational efficiency, we employed therefore 3D periodic boundary conditions but performed simulations both without and with a large vacuum gap perpendicular to the interface ($L_z' = L_z + L_{gap}$, $L_{gap} = 2L_z \approx 8L_x \approx 8L_y$), which is known to reproduce the results of 2D periodic boundary conditions. The results of these two calculations are essentially identical.

The initial amorphous polymer melt was constructed to be of density ~1.0 g/cm^3. The lower density initial state was found to improve the convergence of the equilibration procedure by

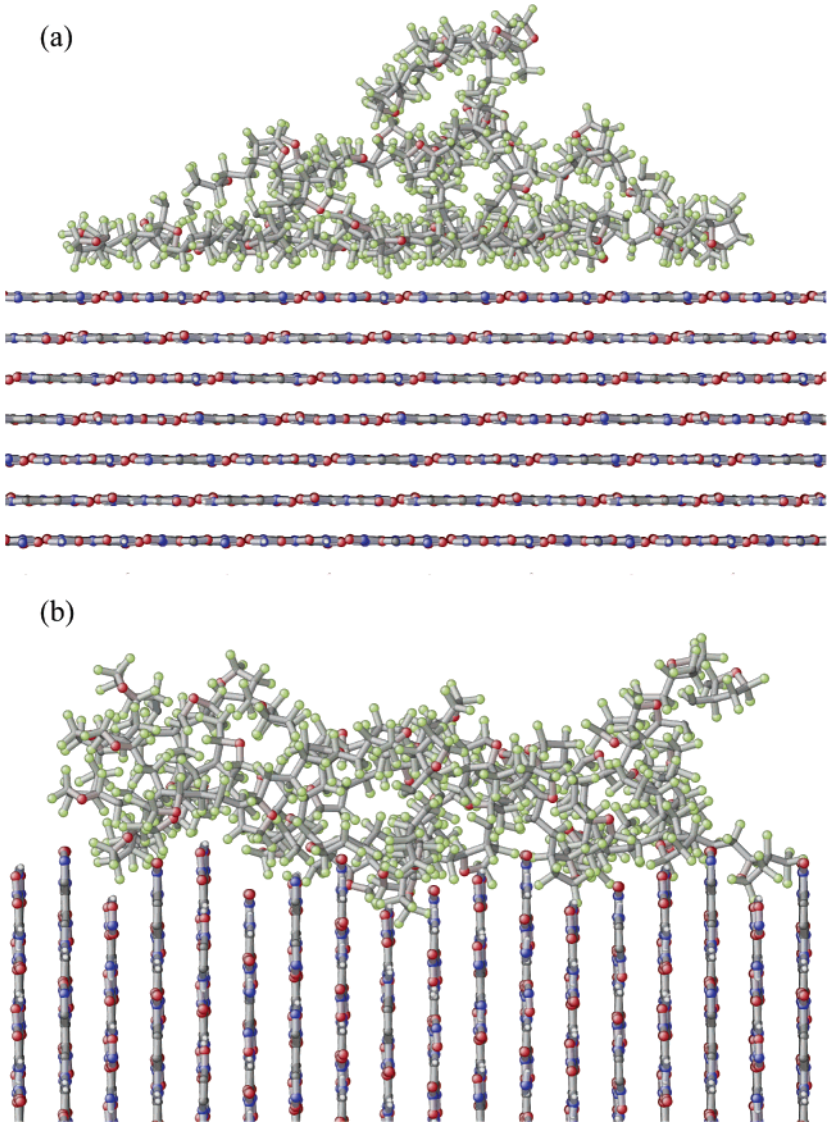

Figure 6. Snapshot of a single Cytop polymer chain geometry at the [001] and [100] TATB surfaces (a and b, respectively) after ~300 ps at 211 K above the polymers T_g. The increased surface area available to the polymer on the [100] TATB surface is apparent.

avoiding close-contact high-energy configurations. All amorphous structures were initially simulated at 550 K under *NPT* conditions. The volume equilibration process was carried out for a minimum duration of 5 ns. Following this step, the systems were cooled in *NPT* runs in increments of 25 K or 50 K and equilibrated for 5 ns each at the desired temperature.

III. Simulation Results and Discussion

a. Amorphous Cells and Force-Field Validation. The computation of the volume−temperature ($V-T$) properties of amorphous AF, obtained from our MD simulations, is shown in Figure 2 for the 15 120-mer chain melt. The $V-T$ results are important for two reasons; first, the results, when compared to experimental data, provide a means of determining the quality of the force-field parameters used in the simulations, and second, it allows for a direct prediction of the volumetric glass transition temperature, T_g, which is of fundamental importance in determining the material properties of the polymer. (Further validation of the force field in terms of its structural and conformational properties may be found in ref 23.) The $V-T$ curve, which shows a distinct break characteristic of vitrification, represents the location of the glass transition temperature. The extraction of the volumetric T_g in this manner is common, although only empirically justified.[23,37−46] The simulation results reveal a T_g which occurs at ~162 °C, as compared to the experimentally determined T_g of 160 °C,[47] while the calculated volumetric coefficient of thermal expansion, $\beta = V_0^{-1}[\delta V/\delta T]_p$, above and below T_g are ~1039 and ~255 ppm/°C, respectively, as compared to the experimental values of 960 and 222 ppm/°C, respectively. Thus, the simulations results are in excellent agreement with experiment and demonstrate the accuracy of the COMPASS[26] force-field parameter set used here. Table 1 summarizes our simulation results for all four polymers and compares with room temperature experimental results, where available. The computed glass transition temperatures and densities for the various fluoropolymers compare well to experiment.

As a further check to the validity of the interaction potentials used here, Table 1 compares the solubility parameters, δ, predicted using the van Krevelen group additive method[48] for the four different fluoropolymers studied here at 300 K, to our computed solubility parameters, where $\delta = (\Delta E/V)^{1/2}$; V is the molar volume, and ΔE is the nonbonded potential energy difference between the bulk melt state and that in which the macromolecules can no longer feel each other. The computed solubility parameters for the various fluoropolymers compare

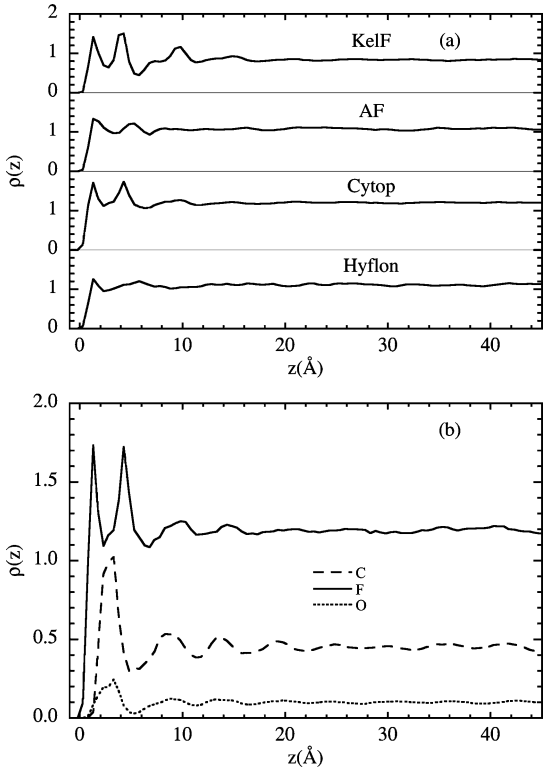

Figure 7. Fluorine density profiles for all polymers studied here at the [001] TATB interface (in density units) at 500 K (a). Panel (b) shows the density profiles for the carbon, fluorine, and oxygen atoms for Cytop polymer at the [001] TATB interface.

well to that predicted by the van Krevelen group additive method.[48] Accurate values for the computed solubility parameter are essential since the polymer cohesive energy directly affects the overall wetting behavior of the polymer when interfaced to a solid substrate.

b. Interfaces and Surface Properties. As mentioned in section II.b, the TATB/fluoropolymer interfaces were constructed by bringing the amorphous fluoropolymer melts close to the TATB interface. An example of such an ensemble is given in Figure 3 for Cytop interfaced to the [001] TATB surface. The potential energy of the interface structures were minimized using MM energy minimization techniques and then subjected to a minimum of 5 ns MD simulations at ~500 K, during which various interfacial properties were monitored.

Of particular interest here is the study of the surface properties, namely, the interfacial tension, γ_{12}, work of adhesion, W_{12}, and spreading coefficient, S. The corresponding microscopic expressions for the interfacial tension for the [001] and [100] TATB/polymer interfaces, written in terms of the pressure tensor,[49−55] are

$$\gamma_{12}^{[001]} = \frac{L_z}{2}\left[p_{zz} - \frac{1}{2}(p_{xx} + p_{yy})\right] \quad (1)$$

$$\gamma_{12}^{[100]} = \frac{L_x}{2}\left[p_{xx} - \frac{1}{2}(p_{yy} + p_{zz})\right] \quad (2)$$

where $p_{\alpha\alpha}$ ($\alpha = x$, y, or z) is the $\alpha\alpha$ element of the pressure tensor and L_z and L_x are the lengths of the simulation cell in the z and x directions, respectively. Other techniques to compute the interfacial tension, which are based on the internal energy contributions, have been implemented by others.[56−58] However, these techniques neglect the "adhesion tension",[59] which has been shown to contribute significantly to γ_{12}.[55] The work of adhesion, W_{12}, is calculated as the difference between the TATB surface tensions, γ_1, the fluoropolymer surface tensions, γ_2, and the interfacial tension, γ_{12}, as

$$W_{12} = \gamma_1 + \gamma_2 - \gamma_{12} \quad (3)$$

The TATB surface tensions, γ_1, for the [001] and [100] surface were computed as the difference in energy between the interfacial structure ($E_{\text{interface}}$) and the TATB bulk energy, E_{bulk}, as

$$\gamma_1 = \frac{E_{\text{interface}} - E_{\text{bulk}}}{2A} \quad (4)$$

where the surface area is $2A$, as two surfaces of area, A, are formed upon the creation of the interface. The various fluoropolymer surface tensions, γ_2, used to compute W_{12}, were obtained from the molar parachors group additive method.[48] To validate the molar parachor surface tension results, a single simulation of a KelF polymer film was performed to compute γ_2. The computed γ_2 from the MD simulation for the KelF film was found to be 28 ± 1 erg cm^{-2}, in excellent agreement with the molar parachor group additive value of 27 erg cm^{-2} (see Figure 4a).

Finally, the spreading coefficient, S, is defined as

$$S = \gamma_1 - \gamma_2 - \gamma_{12} \quad (5)$$

With this definition, positive values of S indicate that the liquid polymer will spread onto the solid surface, while negative values imply that the liquid polymer will contract, and a value of zero means the liquid has no propensity to wet the solid surface. Table 2 shows the values for the computed surface tensions, interfacial tensions, work of adhesion, and spreading coefficients for the four fluoropolymers at each of the two TATB surfaces. The simulation results of the computed interfacial surface tension for both KelF at the [001] TATB interface and of a KelF film consisting of 15 KelF polymer chains are shown in Figure 4. The numerical uncertainty of γ_2 and γ_{12} has been estimated to be ~±2 erg cm^{-2}. The computed work of adhesion, W_{12}, and interfacial tension, γ_{12} show a distinct difference between the two TATB surfaces. The interfacial tension for the [001] TATB surface, $\gamma_{12}^{[001]}$, is positive for all polymers, whereas the interfacial tensions for the [100] surface, $\gamma_{12}^{[100]}$, are all significantly negative. This is also borne out in the computed W_{12} values, where a decrease of the interfacial energy leads to an increase in W_{12}, which are all found to be substantially greater at the [100] TATB surface.

The difference in the interfacial tension between the two TATB surfaces may be attributed to the roughly ~45% increase in the available accessible surface area of the [100] TATB surface as compared to the [001] TATB surface (based on a Connolly surface construction[60,61]), for which the polymer can bind. Furthermore, the pendent $-NH_2$ and $-NO_2$ moieties of TATB which are exposed at the [100] surface may play a role in the overall adhesion properties due to the presence of the dipole−dipole interactions between the $-NH_2$ and $-NO_2$ moieties and the polymer. The rough [100] TATB surface is shown in Figure 5, along with the Connolly accessible surface. To illustrate this point, Figure 6 shows a single Cytop polymer chain geometry after ~0.3 ns *NVT* dynamics following the introduction of the chain to the TATB surface. (Figure 6a shows the geometry at the [001] TATB surface, and Figure 6b shows the geometry at the [100] TATB surface.) As is apparent, the polymer chain at the [100] TATB surface migrates into the

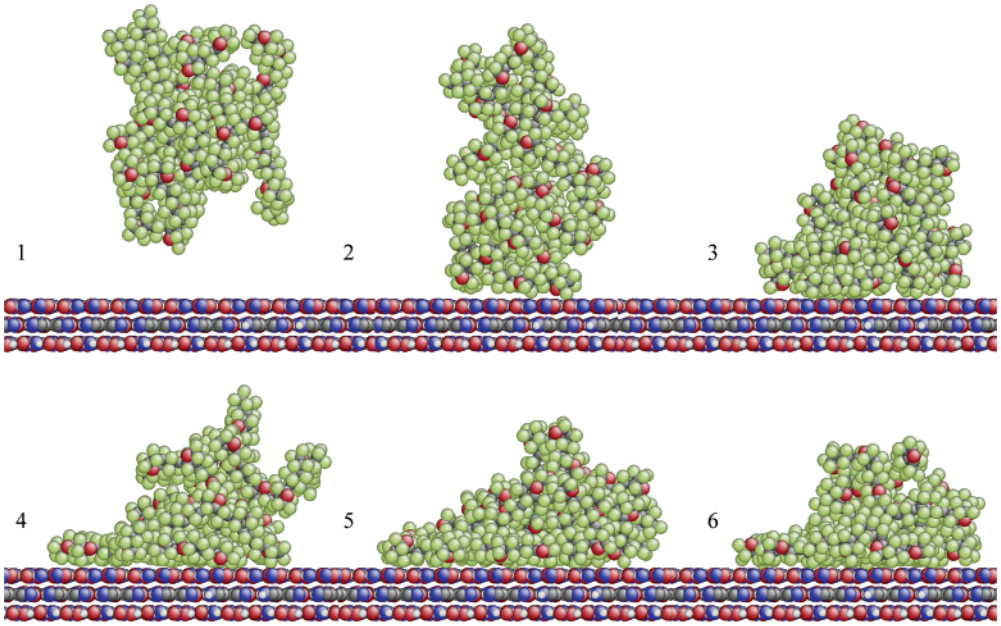

Figure 8. Snapshots of the time evolution of a single Cytop polymer chain at the [001] TATB interface at 60 ps intervals (label 1 = 0 ps; label 2 = 60 ps; label 3 = 120 ps; label 4 = 180 ps; label 5 = 240 ps; label 6 = 300 ps).

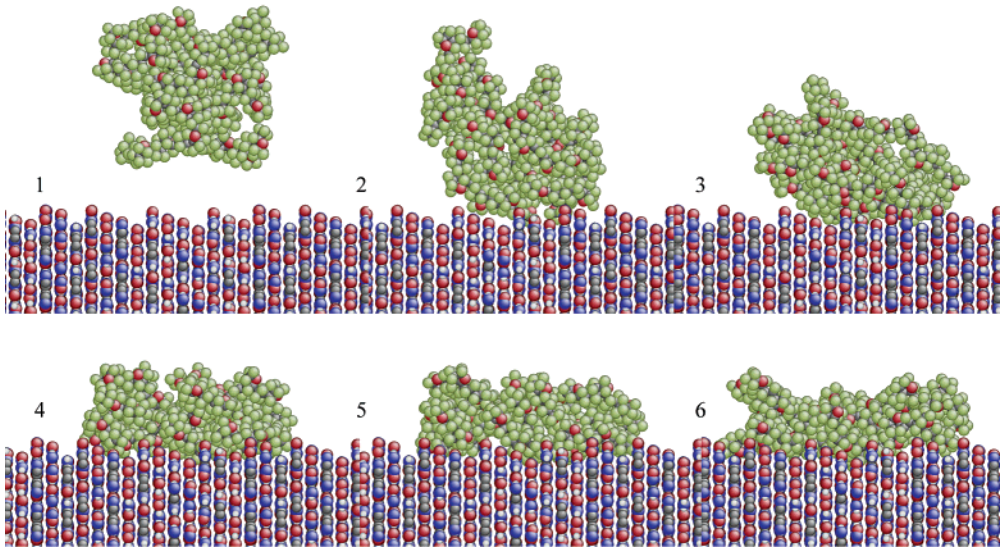

Figure 9. Snapshots of the time evolution of a single Cytop polymer chain at the [100] TATB interface at 60 ps intervals (label 1 = 0 ps; label 2 = 60 ps; label 3 = 120 ps; label 4 = 180 ps; label 5 = 240 ps; label 6 = 300 ps).

rough "cavities" along the surface, in contrast to the relatively "flat" geometry seen along the [001] TATB surface.

The polymers' ability to wet the solid TATB surface is reflected in the computed spreading coefficient, *S*. As seen in Table 2, the computed spreading coefficient, and thus the ability to wet the solid TATB surface, for all polymers, is significantly greater at the [100] TATB surface as compared to the [001] TATB surface. In fact, the computed negative value of the spreading coefficient for Hyflon at the [001] TATB surface suggests that Hyflon does not wet the [001] TATB surface. The weak adhesion seen for Hyflon at the [001] TATB surface could be due in part to the bulky pendent $-O-CF_3$ moiety (see Figure 1c), which effectively inhibits efficient surface packing at the smooth [001] TATB surface.

To further illustrate the diminished wetting of the Hyflon polymer as compared to the other polymers studied here, we monitor the time-averaged density profile of the polymers at both the [001] and [100] TATB surfaces. Figure 7a shows the density variation of the pendent fluorine atoms as a function of interfacial distance from the [001] TATB surface for all polymers studied here. It is found that the fluorine density profile for the Hyflon polymer is relatively structureless, as compared to the other polymers. In contrast, all polymers, except Hyflon, show two distinct peaks close to the [001] TATB interface. The lack of apparent structure of the Hyflon polymer further illustrates the diminished wetting of the Hyflon polymer as compared to the others studied here. Figure 7b shows the time-averaged density profiles for all moieties present in the Cytop polymer for comparison purposes.

As a qualitative measure of the enhanced spreading at the [100] TATB surface as compared to the [001] TATB surface, a single 120-mer Cytop polymer chain was allowed to dynamically evolve for 0.3 ns on each of the [001] and [100] TATB surfaces in 2-dimensional MD simulations. The TATB surface consisted of 4536 TATB molecules (108 864 total TATB atoms) with [001] and [100] TATB surface dimensions of $a = 169.528$ Å $\times$ $b = 140.571$ Å and $b = 140.571$ Å $\times$ $c = 131.868$ Å, respectively. Figures 8 and 9 show the time evolution of the

single Cytop 120-mer polymer chain at the [001] and [100] TATB surface, respectively. It is apparent that the single Cytop polymer chain readily spreads onto both the [001] and [100] TATB surfaces. Qualitatively, however, the polymer at the [100] TATB interface seems to spread more evenly and readily penetrates into the rough [100] TATB cavities.

IV. Conclusion

The focus of this article is on the adhesion properties of fluoro- and perfluoropolymers onto TATB crystal surfaces. To our knowledge, this is the first instance of such a study concerning the novel Cytop, Hyflon, and AF amorphous perfluoropolymers. It was determined that the COMPASS[26] force field used here accurately predicted the volume−temperature behavior of this novel class of polymers. It was found that all polymers studied here except Hyflon have a propensity to readily wet the two TATB surfaces studied. Hyflon wets only the TATB [100] surface. Further, the adhesion onto the [100] TATB surface is significantly favored over adhesion onto the [001] TATB surface mainly due to the increase in the accessible surface area in the former. The current study could be helpful in determining polymeric binders suitable for use with TATB.

Acknowledgment. The work was performed under the auspices of the U.S. Department of Energy by the University of California Lawrence Livermore National Laboratory under Contract W-7405-Eng-48. The project (06-SI-005) was funded by the Laboratory Directed Research and Development Program at LLNL. We thank the Livermore Computing for generous amounts of CPU time on Thunder and MCR clusters.

References and Notes

(1) Lovinger, A. J. *Development in Crystalline Polymers;* Applied Science: London, 1982; Vol. 1.
(2) James, E. *The Development of Plastic Bonded Explosives*; UCRL-12439-T; Lawrence Livermore National Laboratory: Livermore, CA, 1965.
(3) http://www.solvaysolexis.com/Resources.htm#HyflonPFA.
(4) A brochure detailing the technical properties of the Teflon AF 1600 product can be obtained from the Du Pont Corp., Wilmington, DE, No. HO7805.
(5) Sugiyama, N. *Modern Fluoropolymers: High Performance Polymers for Diverse Applications;* John Wiley & Sons: New York, 1997; p 541.
(6) Pruneda, C. O.; Kolb, J. R.; Bower, J. K. *Ind. Eng. Chem. Prod. Res. Dev.* **1980**, *19*, 326−329.
(7) Nie, F. D.; Liu, J.; Li, J. S.; Huang, H.; Zhao, X. P.; Li, Y. S.; Fan, Z. Y. *Acta Chim. Sin.* **2006**, *64*, 2414−2418.
(8) Xu, X. J.; Xiao, H. M.; Xiao, J. J.; Zhu, W.; Huang, H.; Li, J. S. *J. Phys. Chem. B* **2006**, *110*, 7203−7207.
(9) Ma, X. F.; Xiao, J. J.; Huang, H.; Ju, X. H.; Li, J. S.; Xiao, H. M. *Chin. J. Chem.* **2006**, *24*, 473−477.
(10) Xiao, J. J.; Huang, Y. C.; Hu, Y. J.; Xiao, H. M. *Sci. China Ser. B: Chem.* **2005**, *48*, 504−510.
(11) Ma, X. F.; Xiao, J. J.; Huang, H.; Zhu, W.; Li, J. S.; Xiao, H. M. *Acta Chim. Sin.* **2005**, *63*, 2037−2041.
(12) Huang, Y. C.; Hu, Y. J.; Xiao, J. J.; Yin, K. L.; Xiao, H. M. *Acta Phys.-Chim. Sin.* **2005**, *21*, 425−429.
(13) Xiao, J. J.; Gu, C. G.; Fang, G. Y.; Zhu, W.; Xiao, H. M. *Acta Chim. Sin.* **2005**, *63*, 439−444.
(14) Ma, X. F.; Xiao, J. J.; Yin, K. L.; Xiao, H. M. *Chin. J. Chem. Phys.* **2005**, *18*, 55−58.
(15) Roszak, S.; Gee, R. H.; Balasubramanian, K.; Fried, L. E. *Chem. Phys. Lett.* **2003**, *374*, 286−296.
(16) Gee, R. H.; Roszak, S.; Balasubramanian, K.; Fried, L. E. *J. Chem. Phys.* **2004**, *120*, 7059−7066.
(17) Gee, R. H.; Maxwell, R. S.; Balazs, B. *Polymer* **2004**, *45*, 3885−3891.
(18) Goncharov, A. F.; Manaa, M. R.; Zaug, J. M.; Gee, R. H.; Fried, L. E.; Montgomery, W. B. *Phys. Rev. Lett.* **2005**, *94*, 6.
(19) Roszak, S.; Gee, R. H.; Balasubramanian, K.; Fried, L. E. *J. Chem. Phys.* **2005**, *123*, 14.
(20) Maiti, A.; Gee, R.; Maxwell, R.; Saab, A. *J. Phys. Chem. B* **2006**, *110*, 3499−3503.
(21) Zepeda-Ruiz, L. A.; Maiti, A.; Gee, R.; Gilmer, G. H.; Weeks, B. L. *J. Cryst. Growth* **2006**, *291*, 461−467.
(22) Molecular Simulations, Inc., San Diego, CA, 1999.
(23) Gee, R. H.; Fried, L. E.; Cook, R. C. *Macromolecules* **2001**, *34*, 3050−3059.
(24) The [001] and [100] TATB surfaces were chosen to be studied here since they are two of the most prominently expressed TATB surfaces as determined from the Hartman−Perdok crystal growth morphology method [Hartman, P.; Perdok, W. G. *Acta Crystallogr.* **1955**, *8*, 49].
(25) The temperature was chosen so as to be above the glass transition temperatures for all the polymers considered here.
(26) Sun, H. *J. Phys. Chem. B* **1998**, *102*, 7338−7364.
(27) Durig, J. R.; Sheehan, T. G. *Raman Spectrosc.* **1990**, *21*, 635.
(28) Plimpton, S. J. *J. Comput. Phys.* **1995**, *117*, 1−19.
(29) Verlet, L. *Phys. Rev.* **1967**, *159*, 98.
(30) Nosé, S. *J. Chem. Phys.* **1984**, *81*, 511.
(31) Melchionna, S.; Ciccotti, G.; Holian, B. L. *Mol. Phys.* **1993**, *78*, 533.
(32) Allen, M. P.; Tildesley, D. J. *Computer Simulation of Liquids;* Clarendon Press: Oxford, UK, 1989.
(33) Hockney, R. W.; Eastwood, J. W. *Computer Simulation Using Particles;* McGraw-Hill: New York, 1981.
(34) Trokhymchuk, A.; Alejandre, J. *J. Chem. Phys.* **1999**, *111*, 8510.
(35) Chang, J.; Han, J.; Yang, L.; Jaffe, R. L.; Yoon, D. Y. *J. Chem. Phys.* **2001**, *115*, 2831.
(36) Spohr, E. *J. Chem. Phys.* **1997**, *107*, 6342.
(37) Boyd, R. H.; Gee, R. H.; Han, J.; Jin, Y. *J. Chem. Phys.* **1994**, *101*, 788−797.
(38) Gee, R. H.; Boyd, R. H. *Polymer* **1995**, *36*, 1435−1440.
(39) Gee, R. H.; Boyd, R. H. *J. Chem. Phys.* **1994**, *101*, 8028−8038.
(40) Han, J.; Boyd, R. H. *Macromolecules* **1994**, *27*, 5365.
(41) Han, J.; Boyd, R. H. *Polymer* **1996**, *37*, 1797.
(42) Han, J.; Gee, R. H.; Boyd, R. H. *Macromolecules* **1994**, *27*, 7781−7784.
(43) Pant, P. V. K.; J.; H.; Smith, G. D.; Boyd, R. H. *J. Chem. Phys.* **1993**, *99*, 597.
(44) Rigby, D.; Roe, R.-J. *J. Chem. Phys.* **1988**, *89*, 5280.
(45) Boyd, R. H. *Trends Polym. Sci.* **1996**, *4*, 12−17.
(46) Bharadwaj, R. K.; Berry, R. J.; Farmer, B. L. *Polymer* **2000**, *41*, 7209−7221.
(47) Resnick, P. R.; Buck, W. H. *Modern Fluoropolymers: High Performance Polymers for Diverse Applications*; John Wiley & Sons: New York, 1997; p 397.
(48) Bicerano, J. *Prediction of Polymer Properties*, 3rd ed.; Marcel Dekker: New York, 2002.
(49) Zhang, Y. H.; Feller, S. E.; Brooks, B. R.; Pastor, R. W. *J. Chem. Phys.* **1995**, *103*, 10252−10266.
(50) Feller, S. E.; Zhang, Y. H.; Pastor, R. W. *J. Chem. Phys.* **1995**, *103*, 10267−10276.
(51) Croxton, C. A. *Statistical Mechanics of the Liquid Surface;* John Wiley & Sons: Chichester, 1980.
(52) Kirkwood, J. G.; Buff, F. P. *J. Chem. Phys.* **1949**, *17*, 338.
(53) Rowlinson, J. S.; Widom, B. *Molecular Theory of Capillarity;* Clarendon: Oxford, 1982.
(54) da Rocha, S. R. P.; Johnston, K. P.; Westacott, R. E.; Rossky, P. J. *J. Phys. Chem. B* **2001**, *105*, 12092−12104.
(55) Mansfield, K. F.; Theodorou, D. N. *Macromolecules* **1991**, *24*, 4295−4309.
(56) Henry, D. J.; Yiapanis, G.; Evans, E.; Yarovsky, I. *J. Phys. Chem. B* **2005**, *109*, 17224−17231.
(57) Deng, M.; Tan, V. B. C.; Tay, T. E. *Polymer* **2004**, *45*, 6399−6407.
(58) Zhang, Q.; Cagin, T.; van Duin, A.; Goddard, W. A.; Qi, Y.; Hector, L. G. *Phys. Rev. B* **2004**, *69*, 4.
(59) Vanvoorhis, J. J.; Craig, R. G.; Bartell, F. E. *J. Phys. Chem.* **1957**, *61*, 1513−1519.
(60) Connolly, M. L. *Science* **1983**, *221*, 709.
(61) Connolly, M. L. *J. Appl. Crystallogr.* **1983**, *16*, 548.

MA0702501